Nanoscale

Cite this: *Nanoscale*, 2012, **4**, 5659

www.rsc.org/nanoscale

PAPER

Nickel incorporated carbon nanotube/nanofiber composites as counter electrodes for dye-sensitized solar cells

Prakash Joshi,[a] Zhengping Zhou,[b] Prashant Poudel,[a] Amit Thapa,[a] Xiang-Fa Wu*[b] and Qiquan Qiao*[a]

Received 4th June 2012, Accepted 13th July 2012
DOI: 10.1039/c2nr31379k

A nickel incorporated carbon nanotube/nanofiber composite (Ni-CNT-CNF) was used as a low cost alternative to Pt as counter electrode (CE) for dye-sensitized solar cells (DSCs). Measurements based on energy dispersive X-rays spectroscopy (EDX) showed that the majority of the composite CE was carbon at 88.49 wt%, while the amount of Ni nanoparticles was about 11.51 wt%. Measurements based on electrochemical impedance spectroscopy (EIS) showed that the charge transfer resistance (R_{ct}) of the Ni-CNT-CNF composite electrode was 0.71 Ω cm^2, much lower than that of the Pt electrode (1.81 Ω cm^2). Such a low value of R_{ct} indicated that the Ni-CNT-CNF composite carried a higher catalytic activity than the traditional Pt CE. By mixing with CNTs and Ni nanoparticles, series resistance (R_s) of the Ni-CNT-CNF electrode was measured as 5.96 Ω cm^2, which was close to the R_s of 5.77 Ω cm^2 of the Pt electrode, despite the significant difference in their thicknesses: ~22 μm for Ni-CNT-CNF composite, while ~40 nm for Pt film. This indicated that use of a thick layer (tens of microns) of Ni-CNT-CNF counter electrode does not add a significant amount of resistance to the total series resistance (R_{s-tot}) in DSCs. The DSCs based on the Ni-CNT-CNF composite CEs yielded an efficiency of 7.96% with a short circuit current density (J_{sc}) of 15.83 mA cm^{-2}, open circuit voltage (V_{oc}) of 0.80 V, and fill factor (FF) of 0.63, which was comparable to the device based on Pt, that exhibited an efficiency of 8.32% with J_{sc} of 15.01 mA cm^{-2}, V_{oc} of 0.83, and FF of 0.67.

Introduction

Dye-sensitized solar cells (DSCs) have been extensively studied as a prospective alternative to conventional silicon solar cells ever since O'Regan and Gratzel developed cells with a power conversion efficiency of 7.9% using a high surface area-nanocrystalline TiO_2 and ruthenium complex dye in 1991.[1–5] Typical DSCs use a porous network of nano-sized TiO_2 particles, onto which a monolayer of dye molecules is attached. Upon illumination, dye molecules absorb light and inject electrons into TiO_2, which serves as an electron transport medium. Holes, carried by an iodide/triiodide redox electrolyte, move toward the counter electrode, which is usually a platinized fluorine doped tin dioxide (FTO) glass substrate. Electrons from TiO_2 flow through an external load and reach the counter electrode where reduction of triiodide to iodide takes place, completing the electrical circuit. Recently energy conversion efficiency beyond 12% was reported under simulated AM 1.5 global sunlight.[6] This efficiency was achieved using a donor–π-bridge–acceptor zinc porphyrin (YD2-o-C8) with a broad absorption spectrum in combination with $Co^{(II/III)}$tris(bipyridyl)-based redox couple, leading to both high current density (J_{sc}) and open circuit voltage (V_{oc}).

The role of counter electrodes (CE) in DSCs is to reduce triiodide to iodide. Usually, Pt-coated FTO glass substrates serve as the counter electrode. However, Pt is a rare and expensive noble metal and the iodide/triiodide redox couple in the electrolyte is reported to be corrosive to Pt.[7] Low cost carbon-based materials such as carbon black, carbon nanotubes (CNTs), graphite, graphene, carbon nanofibers (CNFs), and poly (3,4-ethylenedioxythiophene) (PEDOT) doped with *p*-toluenesulfonate (PEDOT-TsO) or polystyrenesulfonate (PEDOT-PSS) could exhibit electro-catalytic performance comparable to Pt for reducing I_3^- ions and have been investigated as potential replacement for Pt.[4,5,8–18] Kay *et al.* developed an alternative CE using a carbon catalyst comprised of graphite powder dispersed in carbon black.[7] Imoto *et al.* reported the use of activated carbons to replace Pt and demonstrated comparable device performance to Pt-based DSCs.[9] Bonaccorso discussed different types of CNTs including multi-walled and single-walled CNTs with different chirality as counter-electrodes in DSCs.[19] Calogero *et al.* used a combination of low cost non-purified single-walled CNTs and stainless steel as a counter electrode substrate.[20] Nickel and its composites have also been used as a low cost alternative to replace Pt in counter electrodes.[21–23] Joshi *et al.*

[a]*Center for Advanced Photovoltaics, Department of Electrical Engineering, South Dakota State University, Brookings, SD 57007, USA. E-mail: Qiquan.qiao@sdstate.edu; Fax: +1 605-688-4401; Tel: +1 605-688-6965*
[b]*Department of Mechanical Engineering, North Dakota State University, Fargo, ND 58108, USA. E-mail: xiangfa.wu@ndsu.edu; Fax: +1 701-231-8913; Tel: +1 701-231-8836*

reported the first CNF CEs in DSCs with an efficiency of ~5.4% compared with ~7.0% from Pt CE based devices.[8] The lower efficiency in the CNF based DSCs was mainly attributed to their insufficient surface area for the triiodide reduction.

In this study, a novel composite counter electrode consisting of nickel nanoparticles, CNTs and CNFs (Ni-CNT-CNF composite) was produced and used to replace the expensive Pt in DSCs. The mixture of CNFs and CNTs was expected to significantly increase the surface area for triiodide reduction. Detailed characterization was performed to evaluate the microstructures and the electrochemical performance of the novel CE, which were compared with those obtained from a traditional Pt based DSC. Consequently, the conclusion of this research was the development of a novel low-cost Ni-CNT-CNF CE for use in dye-sensitized solar cells.

Experimental

Preparation of nickel-embedded CNT-coated electrospun CNFs

Polyacrylonitrile (PAN, M_w = 150 000), Nickel(II) acetylacetonate[Ni(AcAc)$_2$, 95%] and *N,N*-dimethylformamide (DMF, 99%) were purchased from Sigma-Aldrich, Corp. St. Louis, MO. Materials were used without further purification.

PAN and Ni(AcAc)$_2$ (ratio 5 : 2 by weight) nanofibers were fabricated by electrospinning. During the process, PAN and Ni(AcAc)$_2$ powders were dissolved in DMF to prepare a 10 wt% electrospinnable solution, which was then placed into a 10 ml plastic syringe installed with a stainless steel spinneret. Electrospinning was performed in a DC electric field of 90 kV m^{-1}, which was generated by applying a positive 18 kV voltage to a 20 cm gap between the spinneret and a grounded nanofiber collector.

The stabilization and carbonization of as-electrospun PAN/Ni(AcAc)$_2$ nanofibers were performed in a tubular quartz furnace. The nanofibers were first annealed at 215 °C for 1 h in air for oxidative stabilization, followed by heating up to 500 °C at a rate of 5 °C min^{-1} in Ar atmosphere. Subsequently, the CNFs were further annealed at 500 °C in a mixed H_2 and Ar (H_2/Ar = 1/2) flow for 1 h to reduce Ni^{2+} to Ni atom. Ni atoms then aggregated onto the CNF surface to form catalytic nanoparticles; these Ni nanoparticles functioned as a catalyst to decompose the hydrocarbon molecules into carbon atoms. Thereafter, the Ni/CNFs were heated up to 900 °C at a rate of 5 °C min^{-1} and annealed for 30 min in Ar flow for complete carbonization. After that, the furnace was cooled down to 650 °C in Ar and maintained at this temperature for 1 h to grow CNTs by introducing a mixture flow of Ar and C_2H_4 (Ar/C_2H_4 = 1).[11]

Electrochemical characterization of Ni-CNT-CNF composites

The chemical composition of the novel Ni-CNT-CNF composite sheets was analyzed by Raman spectroscopy and energy dispersive X-rays spectroscopy (EDX). The Raman spectrum of the Ni-CNT-CNF composite was obtained using a Horiba LabRam HR 800 Raman spectrometer with a laser beam of 532 nm (green laser). An EDX spectrum was obtained using a Hitachi-S3400 N scanning electron microscope (SEM) with an applied bias of 20 KV. The catalytic activity of the Ni-CNT-CNF composite was compared with that of a 40 nm thick sputtered Pt using cyclic voltammetry (CV) and electrochemical impedance spectroscopy (EIS). The CV was carried out in a solution using acetonitrile as a solvent and 10 mM lithium iodide (LiI) and 0.5 mM iodine (I_2) as solutes with 0.1 mM tetrabutylammonium hexafluorophosphate ($(CH_3CH_2CH_2CH_2)_4N(PF_6)$) as a supporting electrolyte. A Ni-CNT-CNF composite coated FTO substrate (or a 40 nm thick sputtered Pt coated FTO substrate), Ag/AgCl, and a Pt wire were used as the working electrode, reference electrode, and counter electrode, respectively. The EIS was carried out using two symmetric dummy cells with a Ni-CNT-CNF composite and sputtered Pt (40 nm thick film) coated FTO as the two electrodes, respectively. The two cells utilized an electrolyte with the same composition as used in real DSCs. An Ametek VERSASTAT3-200 potentiostat with a frequency analysis module (FDA) was used for the EIS measurement. The Nyquist plots were obtained at a zero biased voltage with 10 mV ac and a frequency sweep range from 0.1 Hz to 100 KHz.

Preparation and characterization of Ni-CNT-CNF composite counter electrodes

The original Ni-CNT-CNF composite sheets were crushed into micron-sized pieces, as described in the following. First, the sheets were placed on a polythene net with micron-sized openings (the screen from a screen printer), then the sheets were pressed and rubbed with a pestle. The nanofibers that were pushed through the screen were collected. The paste used to prepare the Ni-CNT-CNF composite CE was made in a plastic vial by mixing 0.1 g of crushed composite with 0.0071 g binder [carboxymethyl cellulose (CMC) sodium salt] in 0.4 ml DI water.[24] The vial was then centrifuged at 10 000 rpm for 30 min. The extracted mixture was manually stirred for about 20 min. Before coating the paste onto the FTO substrates, the mixture in the vial was left unstirred for several hours to thoroughly soak the composite with the binder solution. The paste was then doctor bladed onto the FTO substrates (8 Ω per square, Hartford Glass, 400 nm thick FTO) using a mask with a circular aperture with the diameter ~7.8 mm. To tune the thickness of the CE films, masks with varying thickness were adopted in the course of doctor blading. The coated Ni-CNT-CNF composite films were allowed to dry in air at room temperature until the water in the films evaporated. For better mechanical adhesion on FTOs, the films were mechanically pressed on their surfaces for a few minutes. Finally, the films were baked in air at 60 °C for 12 h in an oven.

Device fabrication and characterization

To prepare photoanodes for solar cells, first a thin layer of compact TiO_2 was coated onto the clean FTO glass substrates. A nanocrystalline TiO_2 (Ti-Nanoxide HT/SP, Solaronix) film was doctor bladed to form a compact layer. The film was left in air for about 10 min, followed by sintering at 475 °C for about 45 min. After that, a TiO_2 light scattering layer (Ti-Nanoxide R/SP, Solaronix) was deposited onto the nanocrystalline TiO_2 and then sintered as described above. The film was then treated with a 40 mM aqueous solution of $TiCl_4$, and sintered again. Finally, the film was cooled down to about 80 °C and then soaked in 0.25 mM of N-719 dye (Solaronix Ruthenizer 535-bisTBA) solution in acetonitrile/valeronitrile (1 : 1 by volume) for 24 h.

The dye-sensitized photoanodes were then washed with acetonitrile to remove any unanchored dye and then dried with compressed nitrogen. The photoanode and Ni-CNT-CNF composite counter electrode were then assembled and sealed using a thermoplastic sealant. An electrolyte containing 0.03 M I_2, 0.60 M BMII, 0.10 M GuSCN, and 0.5 M *tert*-butylpyridine in acetonitrile and valeronitrile (85 : 15 by volume) was injected into the cells.[25] For comparison, similar DSCs based on sputtered Pt CEs were also fabricated as control samples. The devices were tested under simulated sunlight of 100 mW cm^{-2} with an AM 1.5 filter. The area of the cell (photoanode) was 0.16 cm^2.

Results and discussion

Fig. 1(a) and (b) depict the SEM images of the as-prepared CNFs surface-grafted with vapor-grown CNTs. Fig. 1(c) shows a transmission electron microscopy (TEM) image of a single CNF, on which the majority of CNTs were detached by sonication in the course of preparing the TEM samples. Fig. 1(d) and (e) show TEM images of CNTs that were peeled off from the CNF sample by sonication. The black dots in Fig. 1(c) and (d) indicate that the Ni nanoparticles were embedded in both CNFs and CNTs. The Ni nanoparticles on the surface of CNFs functioned as catalysts for the vapor-growth of CNTs. Also, some Ni nanoparticles exist in between the CNTs, indicating different growth mechanisms of CNTs,[26] as shown in Fig. 1(d). The zoomed-in TEM micrograph of these CNTs in Fig. 1(e) shows a multi-walled structure.

Due to weak adhesion between the original CNF sheets and FTO substrate, the CNF sheets were crushed into a paste using a screen printer with micron-sized openings and addition of water and CMC as the binder. The paste was then doctor bladed onto FTO glass as the CE; the microstructure of the paste was characterized by SEM as shown in Fig. 2(a). Compared to the SEM images of the original CNF sheets [see Fig. 1(a) and (b)], no clear CNTs were identified around the CNFs in the final CE film [Fig. 2(a)]. Such observation is due to the fact that the CNTs were peeled off from the CNFs in the course of crushing. Since no materials were lost from the samples during the process, the peeled-off CNTs formed aggregated clusters between the CNFs, as shown in Fig. 2(a). It is well known that CNTs carry excellent electric conductivity and very large specific surface area,[26] which are expected to contribute to the high conductivity and very large

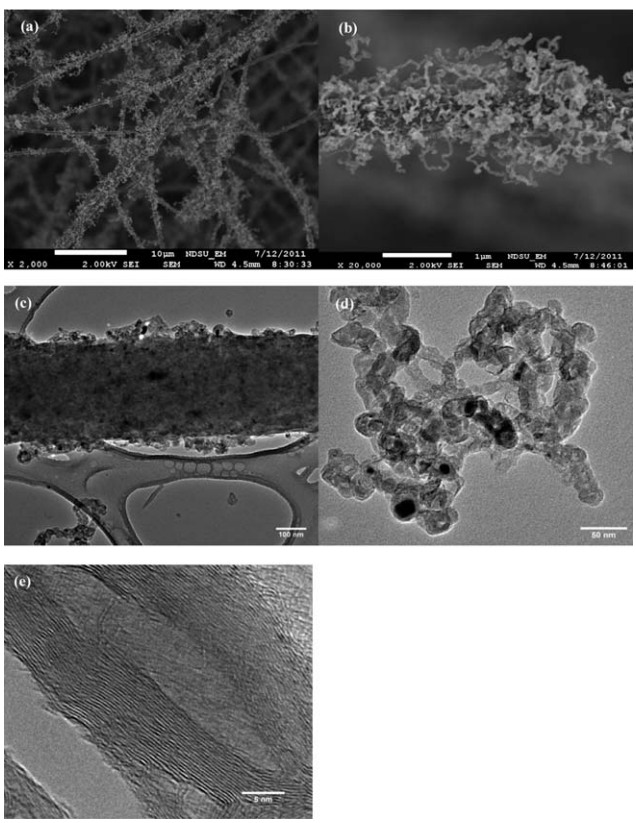

Fig. 1 (a) SEM image of electrospun CNFs surface-grafted with vapor-grown CNTs, (b) SEM image of a typical single CNF surface-grafted with CNTs, (c) TEM image of a typical single CNF with 'roots' of CNTs, (d) TEM image of a Ni-CNT composite peeled off from CNFs, and (e) zoomed CNTs. The black dots in the (c) and (d) are Ni nanoparticles.

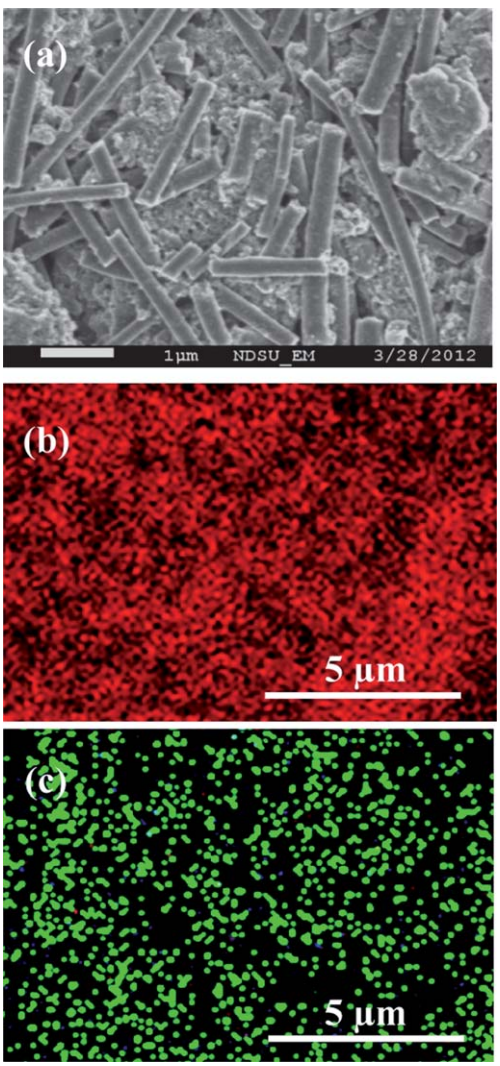

Fig. 2 (a) SEM image of the counter electrode (CE) formed by doctor blading the Ni-CNT-CNF composite paste onto a FTO glass substrate, in which the aggregated clusters between the CNFs are CNTs; (b) energy dispersive X-rays spectroscopy (EDX) mapping of carbon; and (c) EDX mapping of Ni of a typical counter electrode.

surface area of the final CE. In addition, the originally continuous electrospun CNFs were broken into CNF segments with lengths of sub- to micrometers [see Fig. 2(a)] after being deposited as the counter electrode onto the FTO. Compared to the original CNF sheet shown in Fig. 1(a), the shortened CNFs tightly entangled each other, forming a more compact film [see Fig. 2(a)].

Fig. 2(b) and (c) show the EDX mapping of carbon and Ni, respectively. As the voltage applied during the EDX measurement was quite high up to 20 KV, the elements on the surface and in the bulk of the samples could be detected. It can be seen that a majority of the composite CE is carbon with a wt% of 88.49%, while that from Ni nanoparticles was about 11.51% (Table 1). The maps of the carbon and nickel distribution in the CNFs show that nickel is uniformly distributed within the carbon.

Fig. 3 is a Raman spectrum of the original CNF sheet in which CNTs were vapor-grown on the CNF surface using embedded Ni nanoparticles as catalysts. The spectrum consists of a D peak centered at ~1340 cm^{-1} and a G peak centered at ~1575 cm^{-1}. The D peak is due to disordered carbon, and the G peak is from ordered carbon (graphitic structure). The *R*-value (ratio of D peak intensity to G peak intensity) of the Ni-CNT-CNF composite is ~1.12, indicating disordered carbonaceous component is slightly greater than the ordered component of the composite. Disordered carbon is rich in defects. For the Ni-CNT-CNF composites, two types of carbon nanostructures coexist, *i.e.*, the amorphous (disordered) CNFs obtained *via* carbonization of as-electrospun PAN nanofibers (stage 1) and crystalline (ordered) CNTs prepared by chemical vapor deposition (stage 2). The *R*-value basically represents the ratio of these two types of carbon nanostructures. Fig. 1(e) clearly shows that these CNTs have multi-walled structures. Also, due to the unique CNT growth mechanisms, the multi-walled CNTs have multiple kinks & edges, *i.e.*, defects, as can be observed in the zoomed CNT TEM micrograph, which also confirms the sources of the D peak. Trancik *et al.* and Lee *et al.* have reported that defects in CNTs can lead to enhancement of catalytic activity.[27] Hence, disordered carbon might enhance the catalytic activity of the Ni-CNT-CNF composite.

Fig. 4(a) depicts the current density *versus* voltage (*J*–*V*) curves of DSCs based on Ni-CNT-CNF composite and Pt CEs obtained under an illumination of 100 mW cm^{-2} from a solar simulator with an AM 1.5 filter. Table 2 shows the photovoltaic parameters. The DSCs based on Ni-CNT-CNF composite CEs yielded an efficiency of 7.96% with a short circuit current density (J_{sc}) of 15.83 mA cm^{-2}, open circuit voltage (V_{oc}) of 0.80 V, and fill factor (FF) of 0.63. The devices based on Pt CE exhibited an efficiency of 8.32% with J_{sc} of 15.01 mA cm^{-2}, V_{oc} of 0.83, and FF of 0.67. The efficiency of the DSC based on the Ni-CNT-CNF composite CE was nearly equal to the DSC based on Pt CE. The DSC based on the Ni-CNT-CNF composite CE gave a slightly lower V_{oc}, but exhibited an improved J_{sc} compared to the DSC based on Pt CEs. The higher J_{sc} of the Ni-CNT-CNF composite based cells was also observed in the incident photon-to-current conversion efficiency (IPCE) spectral responses, as seen in Fig. 4(b). The total series resistance (R_{s-tot}) of the Ni-CNT-CNF composite CE DSCs, which was obtained from the *J*–*V* curves of the entire cell, was 8.32 Ω cm^2. This was close to the R_s (7.53 Ω cm^2) of the Pt CE devices, even though the thickness of the Ni-CNT-CNF composite CE was much higher (~22 μm) than that of the Pt CE (~40 nm). This indicates that Ni-CNT-CNF composite has a high electric conductivity. The slightly

Table 1 wt% of carbon and Ni in the composite counter electrode

Element	Line	Error 2-sig	Conc.	Units	
C	Ka	6.450	88.49	wt%	
Ni	Ka	2.151	11.51	wt%	
			100	wt%	Total

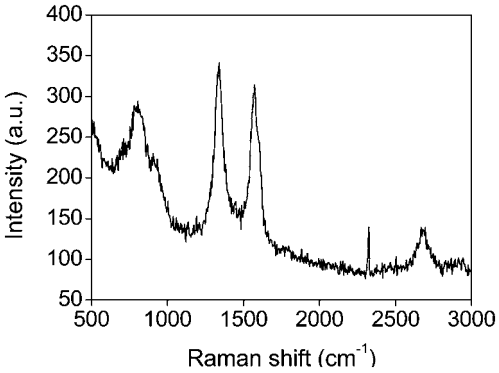

Fig. 3 Raman spectrum of Ni-CNT-CNF composite.

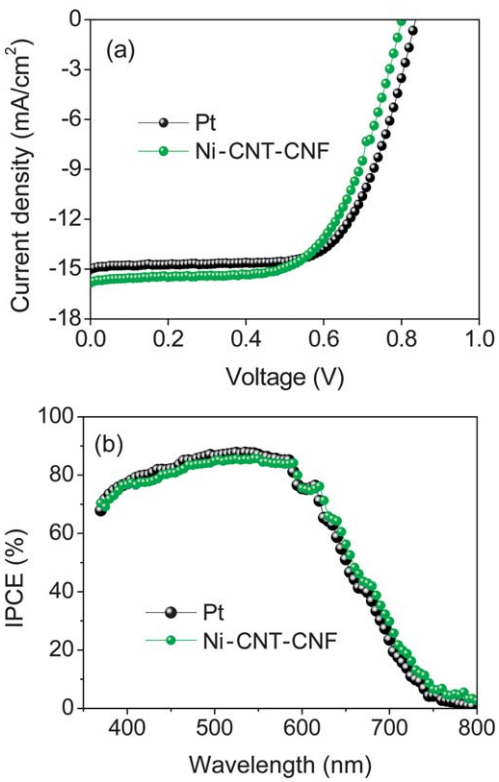

Fig. 4 (a) Comparison of the current density *versus* voltage (*J*–*V*) curves and (b) incident photon-to-current conversion efficiency (IPCE) spectral responses of DSCs based on Ni-CNT-CNF composite CE and Pt CE, respectively.

Table 2 Comparison of photovoltaic parameters of DSCs based on Ni-CNT-CNF composite and Pt CE, respectively (R_{s-tot}: total series resistance of the entire DSCs)

Counter Electrode	J_{sc} (mA cm^{-2})	V_{oc} (V)	FF	η (%)	R_{s-tot} (Ω cm^2)
Ni-CNT-CNF composite	15.83	0.80	0.63	7.96	8.32
Pt	15.01	0.83	0.67	8.32	7.53

increased value R_s of the Ni-CNT-CNF composite cells might have caused the lower FF and efficiency (Table 2).

Fig. 5 depicts the cyclic voltammograms of Ni-CNT-CNF composite and Pt films coated on FTO substrates. The extreme left peaks of each curve were due to the reduction of tri-iodide ions *via* the reaction: $I_3^- + 2e^- = 3I^-$, and the intensity of current density corresponding to these peaks can be regarded as a sign of the catalytic property of the CEs.[9,28] The current densities at the extreme left peaks of the Ni-CNT-CNF composite electrodes in this study were higher than those for the sputtered Pt electrode, indicating that a Ni-CNT-CNF composite can be used as an efficient electrocatalytic material for CEs in DSCs. The Ni-CNT-CNF composite based electrode with a thickness of 16 μm also shows a comparable catalytic property to a sputtered Pt CE for triiodide reduction, and the catalytic capability of the present Ni-CNT-CNF composite was found to increase with an increase in the film thickness.

Fig. 6 shows the Nyquist plots of two symmetrical electrochemical cells. One cell was made up of two identical Ni-CNT-CNF composite electrodes, and the other was made up of two identical sputtered Pt electrodes. Both cells contained an identical electrolyte of I_2 and I^-.

The Nyquist plot for Pt based symmetrical cell exhibited only one arc, but two arcs were observed in the Ni-CNT-CNF composite based symmetrical cell. Murakami *et al.* also reported an additional arc in the Nyquist plot of carbon black based DSCs with zero bias applied for the EIS measurement.[14] According to these, it can be concluded that the first circle originated from solid–solid contact (FTO–carbon or FTO–TiO_2). Furthermore, Roy-Mayhew *et al.* reported two arcs for EIS measurements with a bias of 0.8 V on graphene symmetrical cells, in which they

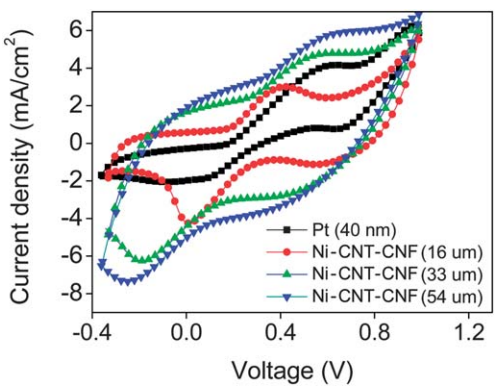

Fig. 5 Cyclic voltammograms (CV) of Ni-CNT-CNF composite films with varying thickness in comparison with Pt film coated on FTO substrates.

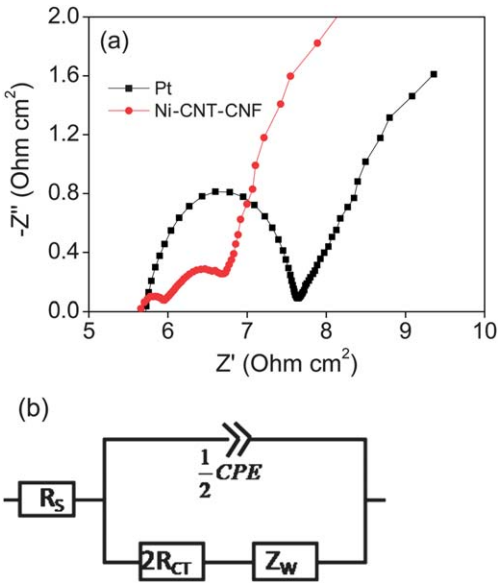

Fig. 6 (a) Electrochemical impedance spectroscopy (EIS) of Ni-CNT-CNF composite and Pt electrodes and (b) equivalent circuit of the symmetrical electrochemical cell used for curve fitting of the Nyquist plots. R_s: the series resistance at the counter electrode; CPE: the constant phase element; R_{ct}: the charge transfer resistance; and Z_w: the Nernst diffusion impedance.

assigned the first arc to be the series resistance (R_s) at the electrode, charge-transfer resistance (R_{ct}) and CPE.[29] The Nyquist plots shown in Fig. 6(a) were obtained from the symmetrical cells at zero bias, which did not contain TiO_2 nanoparticles, but carried the CNTs in the Ni-CNT-CNF composite. As we did not apply any bias voltage in our EIS measurement, interpretation of the behavior at 0.8 V bias by Roy-Mayhew *et al.* should not be considered in our case. The appearance of the first arc can be attributed to the FTO-CNF or FTO-CNTs interface similar to the report by Murakami *et al.* at the zero bias measurement. Hence, the first arc was excluded in order to simplify the curve fitting of Nyquist plots. Fig. 6(b) shows the equivalent circuit used in curve fitting, where the symbols are defined following the standard terminology in the field (R_s: series resistance of the electrodes with Ni catalysts; CPE: constant phase element at the electrode–electrolyte interface; and R_{ct}: charge transfer resistance at the electrode–electrolyte interface; and Z_w: Nernst diffusion impedance).[24] The parameters extracted by fitting the Nyquist plots are shown in Table 3. The charge transfer resistance (R_{ct}) of

Table 3 The parameters extracted by fitting Nyquist plots of the Ni-CNT-CNF composite and Pt electrodes. The area of the film coated with the NiC composite catalyst or Pt catalyst was 0.33 cm^2 and the separation between two electrodes in each symmetrical cell was ~160 μm. Thickness of Ni-CNT-CNF composite and Pt films were ~22 μm and ~40 nm, respectively. R_s: series resistance at the counter electrode; CPE: constant phase element; and R_{ct}: charge transfer resistance

Counter Electrode	R_s (Ω cm^2)	R_{ct} (Ω cm^2)	C (F cm^{-2})	β
Ni-CNT-CNF composite	5.96	0.355	4.372×10^{-2}	0.71
Pt	5.77	0.9	4.82×10^{-5}	0.96

the Ni-CNT-CNF composite electrode was 0.71 Ω cm^2 compared to1.81 Ω cm^2 from the Pt electrode. The small value of R_{ct} of the Ni-CNT-CNF composite indicates a high catalytic activity of the Ni-CNT-CNF composite films. Similarly, the value β for the Ni-CNT-CNF composite was 0.71, while that of the Pt electrode was 0.96. The smaller value of β suggests that the Ni-CNT-CNF composite film is more porous than the Pt film. The porous structure of the Ni-CNT-CNF film can facilitate triiodide penetration deep inside the film, which provides a larger surface area for faster reduction. The value of series resistance (R_s) of the Ni-CNT-CNF composite counter electrode was 5.96 Ω cm^2, close to R_s of 5.77 Ω cm^2 for the Pt electrode despite the significant difference in their thicknesses: ~22 μm for the Ni-CNT-CNF composite, while ~40 nm for the Pt film. This indicates that use of a thick layer (tens of microns) of the Ni-CNT-CNF composite does not yield a significant amount of resistance to the total series resistance (R_{s-tot}) in DSCs.

Conclusion

In summary, a novel Ni-CNT-CNF composite has been synthesized and demonstrated as a low-cost efficient electrocatalyst with lower charge transfer resistance (R_{ct}), larger surface area, and faster reaction rate for reduction of I_3^- into I^- than traditional Pt CE. By blending with CNTs and Ni nanoparticles, the series resistance (R_s) of Ni-CNT-CNF composite CE was 5.96 Ω cm^2, which was close to that of Pt CE (R_s = 5.77 Ω cm^2) despite the significant difference in their thicknesses: ~22 μm for the Ni-CNT-CNF composites in contrast ~40 nm for the Pt films. This suggests that a thick layer (tens of microns) of Ni-CNT-CNF composite CE does not noticeably increase the total series resistance (R_{s-tot}) in DSCs. In addition, the DSCs based on the Ni-CNT-CNF composite CE exhibited comparable photovoltaic performance (J_{sc} = 15.83 mA cm^{-2}, V_{oc} = 0.80 V, FF = 0.63, and η = 7.96%) to those based on Pt CE (J_{sc} = 15.01 mA cm^{-2}, V_{oc} = 0.83 V, FF = 0.67, and η = 8.32%).

Acknowledgements

The study at SDSU was partially supported by the NSF/EPSCoR program (Grant no. 0903804) and by the State of South Dakota, NASA EPSCoR program (Grant no. NNX09AP67A), and SD BoR seed grant. The study at NDSU was partially sponsored by the DoEEPSCoR-Sustainable Energy Seed Grants Initiative Program (SUNRISE).

References

1 B. O'Regan and M. Gratzel, *Nature*, 1991, **353**, 737–740.
2 P. Joshi, L. Zhang, D. Davoux, Z. Zhu, D. Galipeau, H. Fong and Q. Qiao, *Energy Environ. Sci.*, 2010, **3**, 1507–1510.
3 F. Shao, J. Sun, L. Gao, S. Yang and J. Luo, *ACS Appl. Mater. Interfaces*, 2011, **3**, 2148–2153.
4 B. Fan, X. Mei, K. Sun and J. Ouyang, *Appl. Phys. Lett.*, 2008, **93**, 143103.
5 M. X. Wu, X. Lin, T. H. Wang, J. S. Qiu and T. L. Ma, *Energy Environ. Sci.*, 2011, **4**, 2308–2315.
6 A. Yella, H.-W. Lee, H. N. Tsao, C. Yi, A. K. Chandiran, M. K. Nazeeruddin, E. W.-G. Diau, C.-Y. Yeh, S. M. Zakeeruddin and M. Grätzel, *Science*, 2011, **334**, 629–634.
7 A. Kay and M. Grätzel, *Sol. Energy Mater. Sol. Cells*, 1996, **44**, 99–117.
8 P. Joshi, L. Zhang, Q. Chen, D. Galipeau, H. Fong and Q. Qiao, *ACS Appl. Mater. Interfaces*, 2010, **2**, 3572–3577.
9 K. Imoto, K. Takahashi, T. Yamaguchi, T. Komura, J. Nakamura and K. Murata, *Sol. Energy Mater. Sol. Cells*, 2003, **79**, 459–469.
10 A. Kay and M. Gratzel, *Sol. Energy Mater. Sol. Cells*, 1996, **44**, 99–117.
11 S. Burnside, S. Winkel, K. Brooks, V. Shklover, M. Gratzel, A. Hinsch, R. Kinderman, C. Bradbury, A. Hagfeldt and H. Pettersson, *J. Mater. Sci.: Mater. Electron.*, 2000, **11**, 355–362.
12 K. Skupien, P. Putyra, J. Walter, R. H. Kozlowski, G. Khelashvili, A. Hinsch and U. Wurfel, *Progr. Photovolt.: Res. Appl.*, 2009, **17**, 67–73.
13 K. Suzuki, M. Yamaguchi, M. Kumagai and S. Yanagida, *Chem. Lett.*, 2003, **32**, 28–29.
14 T. N. Murakami, S. Ito, Q. Wang, M. K. Nazeeruddin, T. Bessho, I. Cesar, P. Liska, R. Humphry-Baker, P. Comte, P. Pechy and M. Gratzel, *J. Electrochem. Soc.*, 2006, **153**, A2255–A2261.
15 P. Calandra, G. Calogero, A. Sinopoli and P. G. Gucciardi, *Int. J. Photoenergy*, 2010, **2010**, 109495.
16 H. Q. Jiang, S. Sakurai and K. Kobayashi, *Electrochem. Solid-State Lett.*, 2009, **12**, F13–F16.
17 P. Joshi, Y. Xie, M. Ropp, D. Galipeau, S. Bailey and Q. Q. Qiao, *Energy Environ. Sci.*, 2009, **2**, 426–429.
18 A. Hinsch, S. Behrens, M. Berginc, H. Bönnemann, H. Brandt, A. Drewitz, F. Einsele, D. Faßler, D. Gerhard, H. Gores, R. Haag, T. Herzig, S. Himmler, G. Khelashvili, D. Koch, G. Nazmutdinova, U. Opara-Krasovec, P. Putyra, U. Rau, R. Sastrawan, T. Schauer, C. Schreiner, S. Sensfuss, C. Siegers, K. Skupien, P. Wachter, J. Walter, P. Wasserscheid, U. Würfel and M. Zistler, *Progr. Photovolt.: Res. Appl.*, 2008, **16**, 489–501.
19 F. Bonaccorso, *Int. J. Photoenergy*, 2010, **2010**, 727134.
20 G. Calogero, F. Bonaccorso, O. M. Maragò, P. G. Gucciardi and G. DMarco, *Dalton Trans.*, 2010, **39**, 2903.
21 Y. Y. Dou, G. R. Li, J. Song and X. P. Gao, *Phys. Chem. Chem. Phys.*, 2012, **14**, 1339–1342.
22 R. Bajpai, S. Roy, N. kulshrestha, J. Rafiee, N. Koratkar and D. S. Misra, *Nanoscale*, 2012, **4**, 926–930.
23 Q. W. Jiang, G. R. Li, S. Liu and X. P. Gao, *J. Phys. Chem. C*, 2010, **114**, 13397–13401.
24 W. J. Lee, E. Ramasamy, D. Y. Lee and J. S. Song, *ACS Appl. Mater. Interfaces*, 2009, **1**, 1145.
25 S. Ito, P. Liska, P. Comte, R. Charvet, P. Pechy, U. Bach, L. Schmidt-Mende, S. M. Zakeeruddin, A. Kay, M. K. Nazeeruddin and M. Gratzel, *Chem. Commun.*, 2005, 4351–4353.
26 D. M. Guldi, *Phys. Chem. Chem. Phys.*, 2007, **9**, 1400–1420.
27 J. E. Trancik, S. C. Barton and J. Hone, *Nano Lett.*, 2008, **8**, 982–987.
28 L.-Y. Chang, C.-P. Lee, K.-C. Huang, Y.-C. Wang, M.-H. Yeh, J.-J. Lin and K.-C. Ho, *J. Mater. Chem.*, 2012, **22**, 3185–3191.
29 J. D. Roy-Mayhew, D. J. Bozym, C. Punckt and I. A. Aksay, *ACS Nano*, 2010, **4**(10), 6203–6211.

